Integrated-Antenna Over-the-Air Testing for Millimeter-Wave Applications: An Overview of Systems and Uncertainty

Imee Ristika Rahmi Barani, Laurens A. Bronckers, and Adrianus C.F. Reniers

Recent wireless communication systems, including the 5G communication New Radio (NR) operating in the millimeter-wave (mm-wave) bands, demand performance measurements using an over-the-air (OTA) test instead of using the traditional conducted methods. This article provides an overview of various OTA measurement systems that measure the integrated antenna inside a 5G-and-beyond mm-wave device, including the direct far-field (DFF), indirect FF (IFF), near-field (NF), and midfield measurements. By considering several significant parameters, including minimum measurement distance required, metrics that can be measured, and complexity of the electrical and mechanical components of the system, suitable OTA measurement methods for integrated antennas can be selected. Furthermore, factors contributing to the measurement uncertainty of OTA systems based on the technical report (TR) of the 3rd Generation Partnership Project (3GPP) are summarized and discussed. By analyzing the significant parameters of each OTA system and contributors of the measurement uncertainty, the reader can determine the OTA method that is most suitable to measure the integrated antennas for mm-wave communications.

Digital Object Identifier 10.1109/MAP.2022.3195469
Date of current version: 6 October 2022

EDITOR'S NOTE

Xiu Yin Zhang

In this issue's "Measurements Corner" column, the authors provide an overview of various over-the-air (OTA) measurement systems, including direct far-field, indirect far-field, near-field, and midfield measurements, which measure the integrated antenna inside a 5G-and-beyond millimeter-wave device. In addition, factors contributing to the measurement uncertainty of OTA systems are discussed and summarized. By considering significant parameters, including the measurement distance, complexity of setup configuration, desired metrics, and uncertainty contributors of each system, a framework is provided to select the most suitable OTA measurement method for a particular integrated antenna.

INTRODUCTION

Recent wireless communication systems, including 5G NR, utilize mm-wave spectrums that offer wide bandwidth for higher data rates and spectrum efficiencies. The short wavelengths associated with mm-wave bands lead to a smaller antenna size, which is integrated with the RF transceiver system in a compact module [1]. The antenna connectors are not accessible, which makes the conventional conducted performance test methods not applicable [2]. Therefore, the performance evaluation of 5G-and-beyond mm-wave devices requires a different approach by using OTA testing methods [3].

OTA tests have been standardized by the 3GPP and the Cellular Telecommunication and Internet Association to evaluate the user-equipment (UE)-radiated performance of 2G, 3G, and 4G systems [4], [5]. For OTA conformance testing of 5G NR Frequency Range 2 mm-wave devices, the 3GPP released TR 38.810 [6]. It is specified that different test methods such as DFF, IFF, and NF systems are permitted to test different devices under test (DUTs).

An overview of various OTA test methods is discussed in [7]. Different approaches are described to create a realistic propagation environment, including radiated two stages (RTSs), a multiprobe anechoic chamber (MPAC), and reverberation chamber measurement. However, the discussion is only

1045-9243/22©2022IEEE

intended for multiple-input/multiple-output application of the 3G Universal Mobile Telecommunication System and 4G long-term evolution (LTE). The feasibility of RTS and MPAC methods for 5G mm-wave OTA testing is evaluated in [8]–[10]. In [9] and [10], the 3GPP's proposed methods for mm-wave OTA testing, including DFF, IFF, and NF tests, are also examined. The challenges of OTA testing, along with the measurement uncertainty, are introduced. Critical components for the uncertainty of OTA measurements are discussed in [10]. However, the analysis focuses on only the chamber and absorber designs. The 3GPP TR [6] for the proposed methods of mm-wave OTA testing is assessed in [11]. In addition, the discussion on measurement uncertainty is limited.

This article provides an overview of various OTA mm-wave measurement systems, with uncertainty contributors in each. The measurement for RF probe-fed mm-wave antennas is also reviewed to give an overview of the integrated antenna measurement, for example, antenna-in-package (AiP) and antenna-on-chip (AoC). This article provides useful considerations for the measurement community when searching for an OTA solution for integrated antennas by considering relevant parameters of each OTA measurements system, such as the measurement distance, complexity of setup configuration, and desired measured parameters.

OTA MEASUREMENT

The term *OTA* was first introduced in 2006 to describe [12] "a measurement of a full-production device in a practical application."

Some of the significant figures of merit obtained from OTA measurements are [13]

- total radiated power (TRP)
- effective isotropic radiated power (EIRP)
- total isotropic sensitivity
- effective isotropic sensitivity (EIS)
- data throughput and bit error rate.

OTA measurements may include other components such as a base station emulator to generate the communication protocol, and a channel emulator to emulate realistic channel propagation. The scope of this type of OTA measurement is illustrated on the left side of Figure 1. In this article, we focus on OTA measurements that evaluate the performance of a device with an integrated antenna, such as a phased-array antenna. The scope of the integrated-antenna OTA measurement is illustrated on the right side of Figure 1. One of the differences between the two tests is the propagation environment. Currently, the integrated-antenna OTA test is mainly performed in an anechoic environment.

OTA measurements for mm-wave antennas in an anechoic environment have been performed using different methods. For example, the characterization of an mm-wave active phased-array antenna is performed in an anechoic chamber with a planar scanner, as discussed in [14]. In [15] and [16], an FF measurement, which is used to evaluate the RF parameter of an array antenna, is performed with minimum distance inside a compact chamber. In [17], an mm-wave device with an antenna array is measured using the compact antenna test range (CATR) technique. The CATR method is also applied to characterize a 28-GHz AiP module in [18].

OTA MM-WAVE MEASUREMENT SYSTEMS

Measurement of the electromagnetic field radiated by an antenna can be classified into three regions: reactive NF,

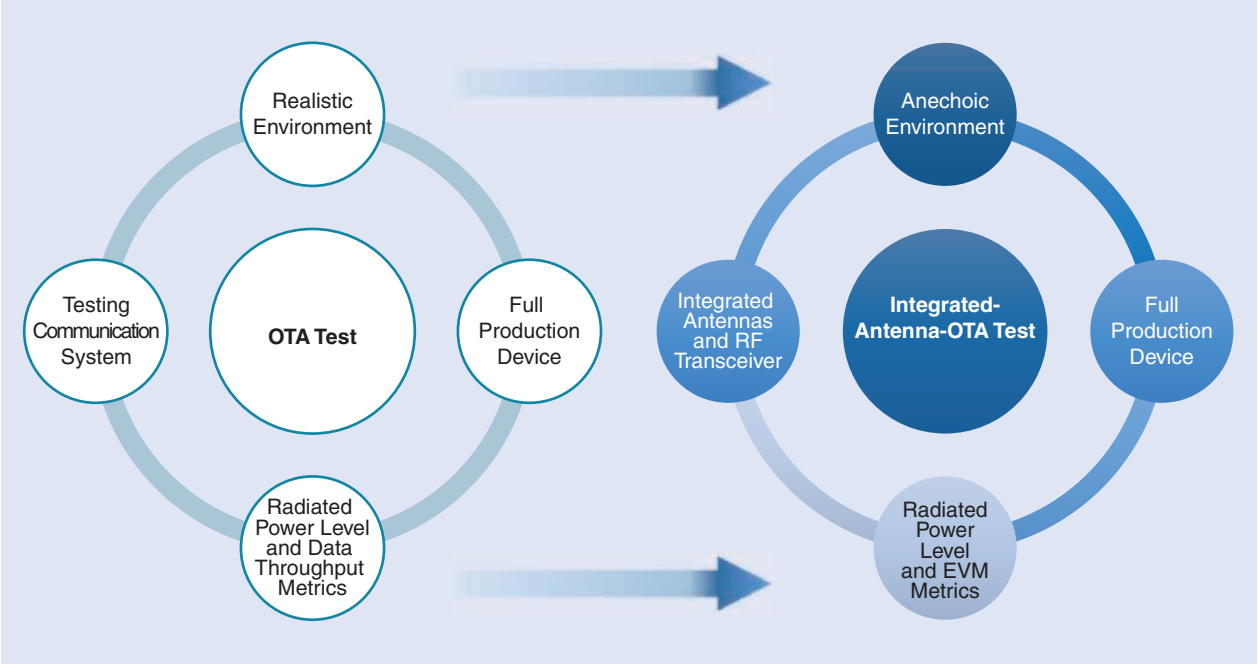

FIGURE 1. The scope of the OTA test and integrated-antenna OTA test. EVM: error vector magnitude.

radiating NF, and FF, as illustrated in Figure 2 [19]. In the reactive NF region, the amplitude fields decay with distance (r) as $1/r^3$. The measurement cannot be performed due to strong coupling. Meanwhile, in the radiating NF region, the radiating NF amplitudes fall off as $1/r^2$. The angular field distribution is dependent on the distance, and the wave shows a strong deviation from plane waves. In this region, by precisely measuring the magnitude and the phase of the electromagnetic field, the obtained measurement results can be transformed afterward into an FF pattern.

In the FF region (often called the *Fraunhofer region*), amplitudes of the FF components decay as $1/r$. The angular field distribution is independent of the distance, and the electromagnetic field can be considered approaching a plane wave. In the following sections, the feasibility, advantages, and disadvantages of several antenna measurement systems related to the field regions in Figure 2 are discussed for integrated-antenna OTA measurements.

DFF MEASUREMENT SYSTEM

In the FF region, an infinite distance is assumed to achieve a plane wave consisting of parallel waves with a constant phase. However, it is not possible due to limited available space and energy. Therefore, to estimate the minimum FF distance, the equation in Figure 2 is frequently used [19]. The following assumptions are made:

- The antenna is a point source.
- The maximum phase deviation is 22.5°.
- D is the largest antenna dimension.

However, determining D is not always straightforward. As an example, for a microstrip patch antenna array, D could be the diagonal diameter of the patch or of the printed circuit board (PCB), which would make an enormous difference depending on the size of the PCB. In another case, if multiple antenna arrays are embedded in one device, the determination of D is more complicated. According to the black-box approach of the 3GPP, the largest dimension of the device is taken [6]. This approach would also support the measurement of an antenna with the chassis-excitation mode.

Figure 3 shows the typical OTA measurement setup of an FF system in an anechoic chamber. It comprises a probe or measurement antenna, the DUT, positioning system, vector network analyzer (VNA) or spectrum analyzer, and data processing system. The DUT is mounted on a positioning system where measurement results for both azimuth and elevation angles can be obtained. An important condition for this measurement method is that the DUT is placed in the center of the quiet zone and aligned to the probe antenna. The quiet zone is the area in which the uniform planar wave is assumed with minimum distortion from the environment and should be covering the radiating elements of the DUT [6]. If multiple antenna elements are measured, or the position of the antenna element is unknown (black box), an error due to the misalignment could arise [20].

By using the DFF method, the EIRP, TRP, EIS, and error vector magnitude (EVM) can be evaluated. However, it is often impractical to measure a large DUT operating at mm-wave frequencies in the DFF measurement system. The minimum FF distance becomes too large, making the needed size of the anechoic chamber not feasible. For example, a 5G mm-wave smartphone with the largest dimension of 15 cm would require a minimum distance of 4.2 m at 28 GHz. Additionally, such a long measurement distance would generate a large free-space path loss (FSPL) of approximately 73.9 dB, which would be problematic for a system with a limited dynamic range [6]. The DFF OTA

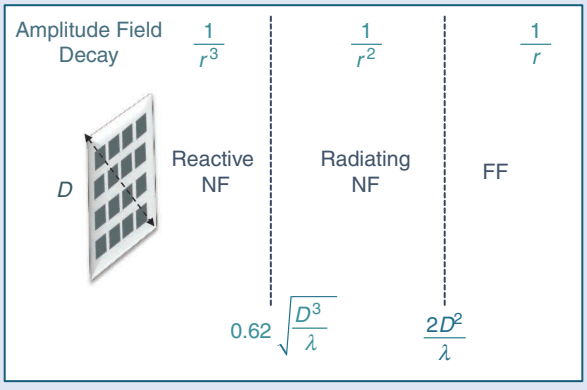

FIGURE 2. The three electromagnetic field regions surrounding the antenna: reactive NF, radiating NF, and radiating FF.

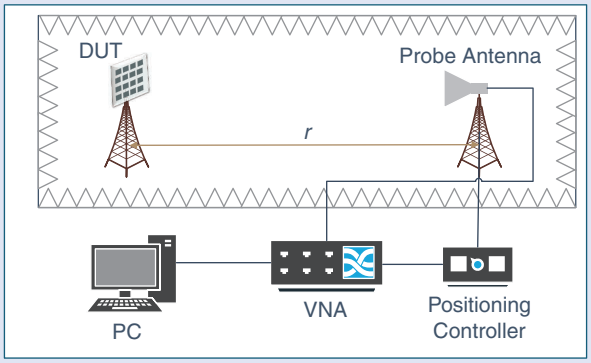

FIGURE 3. A typical OTA measurement setup of the FF system in an anechoic chamber. VNA: vector network analyzer.

measurement is more suitable for mm-wave devices with a small radiating aperture of fewer than 5 cm for operation at 28 GHz [6]. The advantages and disadvantages of the DFF method are summarized in Table 1.

IFF MEASUREMENT SYSTEM

We define the IFF measurement system as *an FF measurement system using collimating component to reduce the minimum distance between antennas*. This method is suitable for DUTs with a large radiating aperture for mm-wave operation, unlike a DFF [6]. One type of IFF approach is the CATR, which uses a parabolic reflector as the collimating element [21]. Figure 4 depicts the measurement configuration of the CATR. The feed antenna is in the focus point of the parabolic reflector and transmits the spherical wave, which is transformed by the parabolic reflector to a plane wave. The area in which the uniform plane waves are created is the quiet zone of the CATR. The size of the quiet zone is typically 50–60% of the reflector size [22]. A CATR with a larger quiet zone at 70% of the reflector size is designed in [23] with the support of feeding mirrors as subreflectors. The measurement distance in the CATR system is roughly 3.5 times the reflector size [6].

Characterization of the quiet zone of the CATR for mm-wave application is described in [24] with the following specifications:

- amplitude ripple: 1 dB
- amplitude taper: 0.5 dB
- phase variation: 10°.

This makes the CATR suitable for black-box measurements as it is relatively unaffected by misalignment of the antenna.

The parabolic reflector is an essential component in a CATR system, which requires meticulous design, production, and maintenance. The surface accuracy of the reflector determines the highest operating frequency of the CATR, and the edges of the reflector determine the lowest operating frequency [25]. At high frequencies, the reflector's surface determines the phase distortion. The low frequency limit is usually encountered when the serrated reflector is approximately 25–30 λ in diameter [26]. The serrated parabolic reflector has overcome the traditional low frequency limit to 16 λ by utilizing some of the techniques in [27].

Ideal plane waves can be generated in the quiet zone of the CATR if the parabolic reflector has a perfect surface and an infinite size. Also, the feed antenna must be in the focus point of the reflector. However, such perfect conditions are impractical to achieve. Even the smallest deviation could cause amplitude taper and phase variation in the quiet zone. In addition, the parabolic reflector also contributes a degree of cross polarization into the system [28]. A proper design is required to improve cross-polarization isolation.

With the CATR system, measurements of EIRP, TRP, EIS, and EVM can be obtained [6]. The main advantage of this system is the lower FSPL due to the smaller FF distance compared to the DFF measurement system. However, obtaining a low uncertainty with an IFF OTA measurement system is challenging [15]. For some cases, several factors may lead to reduced performance of the quiet zone in the IFF compared to a well-calibrated DFF system. The advantages and disadvantages of the CATR system are listed in Table 2.

Besides parabolic reflectors, lenses can be used as elements to create plane waves by diffraction. The operating frequency of the system depends on the dimension and weight of the lens.

TABLE 1. THE ADVANTAGES AND DISADVANTAGES OF A DFF OTA MEASUREMENT.

Advantages	Disadvantages
• measurement setup is easy to configure • measures continuous-wave and modulated signals.	• large measurement distance for mm-wave DUT measurement with black-box approach • high path loss for long measurement distance.

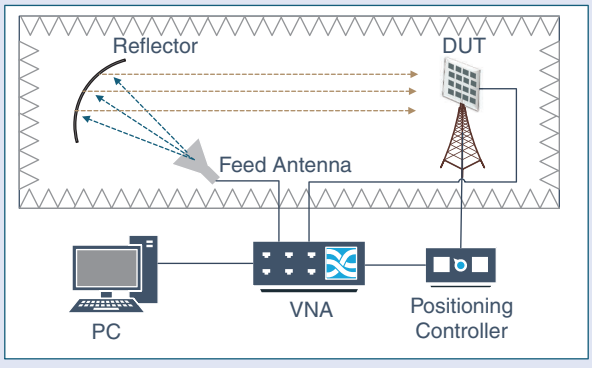

FIGURE 4. The configuration of the compact antenna test range measurement system with a parabolic reflector as the collimating element.

TABLE 2. THE ADVANTAGES AND DISADVANTAGES OF A CATR SYSTEM.

Advantages	Disadvantages
• smaller distance than DFF • measures continuous-wave and modulated signals.	• requires a high-quality parabolic reflector and precise alignment.

The lens-type IFF OTA measurement system is used for the mm-wave applications in [29]. In addition, the use of a hologram-based CATR is studied in [30]. The planar hologram is used as a collimating element with low cost and relatively easy manufacturing. In [31], a hologram CATR is used for wideband operation. However, the strong frequency and polarization dependence of a hologram CATR is still a challenge [32].

A printed reflectarray or transmitarray is also used in the CATR system to create plane waves with a low profile, low cost, and easy manufacturing [33]. The quiet zone is evaluated from the NF of the reflectarray. In [34], the quiet-zone performance of a reflectarray CATR is improved by controlling the aperture disturbance field, including the specular reflection and edge diffraction.

Another technique for IFF measurements is to create plane waves using a plane-wave convertor (PWC) [35]. This method has been simulated to measure 5G mm-wave devices [36]. Instead of employing a parabolic reflector, an active antenna array system is used for a PWC. Multiple elements of the antenna array transmit the spherical wave signals simultaneously. The amplitude and phase weights of each element are adjusted to create plane waves in the quiet zone. Therefore, the efficiency and quality of calculating the amplitude and phase weights of each element have a major influence on the performance of the quiet zone. A fast synthesis approach to handling system complexity is described in [37]. Although a PWC has similar measurement capabilities as a CATR, the complex design of an active-array antenna system is a major challenge.

NF MEASUREMENT SYSTEMS

NF measurements are another solution for measurements in a spatially limited range [38]. It is performed in the radiating NF region (see Figure 2). A separation between the probe and the DUT is typically roughly 3–5 λ of the measuring frequency [39]. The configuration of an NF measurement system is shown in Figure 5. The probe scans over the surface surrounding the DUT to sample the magnitude and phase of the field at discrete points in space. An NF-to-FF transformation must be applied to the measurement data.

The time required to perform an NF scan depends on the type of scanning (see Figure 6), spatial resolution, DUT size, and frequency. Three scanning types, with their unique sampling points, are used: planar, cylindrical, and spherical, as displayed in Figure 6. The selection of scanning depends on the type and directivity of the DUT. Different scanning approaches lead to different complexities in the mechanical system and the analytical or numerical transformations. In addition, the measured NF results are influenced by the probes. Therefore, a probe correction must be applied, and the position of the DUT must be known. This requires an exceedingly small positioning error from the scanner or positioner [40].

Measuring with modulated signals using an NF measurement technique is

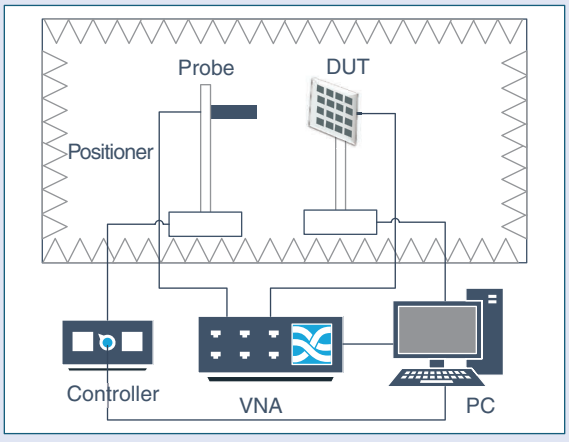

FIGURE 5. The configuration of an NF measurement system.

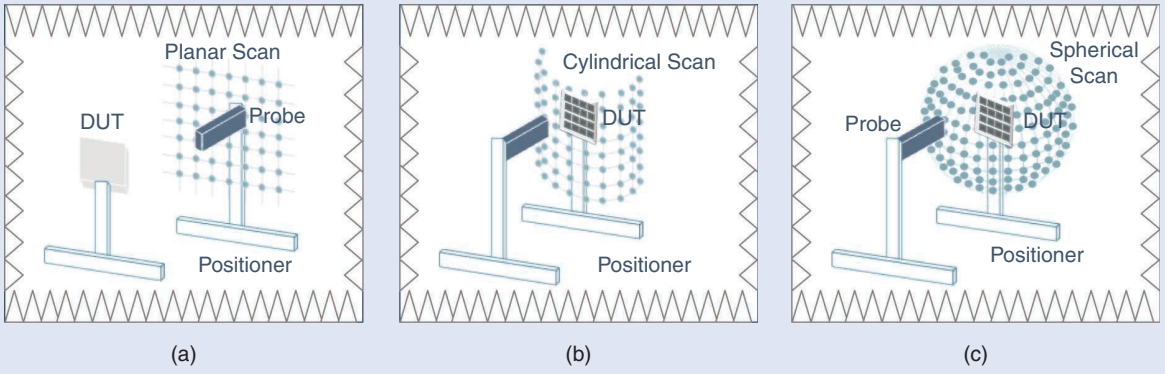

FIGURE 6. Three scanning coordinates with the sampling grids for NF measurement system. (a) The planar, (b) cylindrical, and (c) spherical scanning systems.

challenging, especially when considering how to apply the NF transformation method to derive the FF result of a modulated signal as the theory is based on a continuous-wave signal. Based on 3GPP TR 38.810 [6], the NF measurement system is acceptable for DUTs having a small aperture of the radiating elements to measure the EIRP and TRP for operation at mm-wave. The advantages and disadvantages of an NF system are detailed in Table 3, and we now discuss the three different NF scanning methods in more detail.

PLANAR NF SCANNING

In the planar NF scanning technique, the amplitude and phase are retrieved by moving the probe or the DUT in the *x-y* plane, as shown in Figure 6(a). The area of the scanning aperture should be large enough to receive significant energy from the DUT and minimize the truncation error. If the scanning range is insufficient, the computed radiation pattern could deviate from the FF result [41]. Additionally, the choice of window type for the Fourier transform affects the FF result. The postprocessing of the planar NF method is the least complex of the three methods. However, for measurements using a black-box approach, NF scanning is less accurate than a CATR [17]. Therefore, prior information about antenna position is preferable.

CYLINDRICAL NF SCANNING

In the cylindrical NF scanning technique, the probe is moved at different heights of the cylindrical surface, while the DUT is rotated, as shown in Figure 6(b). By scanning in a cylindrical surface, the exact azimuth pattern can be obtained, but the elevation pattern is limited due to truncation of the scanning aperture. The measurement of mm-wave antennas using cylindrical NF scanning is performed in [42]. Additional mode-filtering techniques can be employed to suppress the reflection from surrounding equipment.

It should be noted that the scanning surface of the planar and cylindrical NF measurements is limited. An estimation of the pattern using an equivalent magnetic current approach to obtain the pattern outside of the limited region is studied in [43]. However, large computational resources are required to solve the integral equations, especially for an electrically large DUT. Another approach is to rotate and measure the DUT in different planes and combine them to increase the valid region [44]. However, it requires additional measurements by moving the probe orthogonal to the conventional scan plane. Extending the region is also done by using an iterative algorithm to extrapolate the valid region of the FF pattern [45].

SPHERICAL NF SCANNING

In the spherical NF scanning technique, several scanning configurations can be applied. One of them is to have the probe fixed while the DUT is moved in spherical coordinates to collect data, as presented in Figure 6(c). If there is no mechanical obstruction, this method can be used to measure the full 3D radiation pattern of the DUT. A multiprobe spherical scanning approach is used in [46] to reduce scanning time. However, with the increased number of probes, the complexity of the design, manufacture, and calibration are challenging.

Another challenge in the NF system is the phase measurement. To reduce the effect of probe-positioning errors on the phase measurement, a phaseless mm-wave measurement is performed in [40] and [47] by using the iterative Fourier technique of two sampling surfaces at different distances from the DUT. However, scanning more surfaces increases the time needed for testing and postprocessing. Modified holographic and time-filtering methods are improved upon for the antenna phaseless measurement in [48]. A phaseless measurement approach based on a digital holographic reconstruction algorithm is proposed in [49] to increase efficiency by having one measurement surface.

TABLE 3. THE ADVANTAGES AND DISADVANTAGES OF AN NF SYSTEM.

Advantages	Disadvantages
• smallest measurement distance • planar scan: suitable for high-gain antennas and is least complex for postprocessing • cylindrical scan: suitable for fan-beam antennas • spherical scan: suitable for any antennas.	• long scanning time • requires high precision of electrical and mechanical components • measures only continuous-wave signals.

MIDFIELD MEASUREMENT SYSTEM

To reduce the measurement distance of the DFF system, the principle of Fraunhofer distance is revisited in [16] and [50]. A different criterion of the FF region, that of observing the antenna's directivity, is used, rather than the device's dimension. By implementing this criterion, DFF measurements are conducted in a much shorter distance if only the peak beam region is analyzed, rather than the full radiation pattern. For a 15-cm DUT at 43 GHz, the measurement distance can be reduced from 6.5 (Fraunhofer distance) to 1.74 m [16].

Another way to measure the phased-array antenna in a short distance is proposed in [15] and [51]. In this method, the midfield is defined as *the range where the probe antenna is in the FF of the individual antenna element but the NF of the phased-array antenna module*. It is observed that within a reasonable distance, the beam pattern of the main lobe has the same direction as the FF, but the EIRP and EIS have an offset depending on the distance, array size, and beam direction.

The offset in the midfield is corrected by a correction factor to obtain the FF result. The correction factor is calculated from the ratio of linear superposition of individual antenna elements in the midfield and FF distances. The correction factor depends on the individual element's position, beamforming coefficient, and probe antenna pattern. The midfield to FF correction can derive results for the main lobe and sidelobes, but not the nulls. Besides, a midfield measurement cannot obtain the depth

of the nulls accurately [15]. The advantages and disadvantages of the midfield method are summarized in Table 4.

OTA MEASUREMENTS USING AN RF PROBE

Due to the use of higher frequencies, integrated antennas such as AoC and AiP are increasingly utilized for 5G mm-wave applications. A measurement to evaluate integrated circuit design is commonly performed during the development phase of the product. In this application, the antenna measurement cannot be conducted in the usual manner with an RF connector, but instead, an RF probe is applied to evaluate the performance of integrated antennas [52].

The RF probe-fed measurement is typically done in a specially designed measurement setup [53]. At the Eindhoven University of Technology, this measurement is conducted in a compact portable mm-wave anechoic chamber [54]–[56], as shown in Figure 7. The chamber has the following properties:

- performs FF, planar, and spherical NF measurements
- provides modular probe holder and probe station for RF probe-fed antenna measurements
- equipped with a camera for alignment validation
- supports movements in the spherical coordinate system.

As depicted in Figure 7, the DUT is positioned in the middle of the chamber in a mechanically stable area where the scan arm is moving around the DUT. In contrast to the RF connector, an RF probe is not fixedly positioned on, for example, a PCB. The construction of an RF probe requires a probe holder to allow the RF probe to be placed on the PCB, creating an RF connection. It is the probe holder that prevents the RF cable from exerting mechanical stress on the RF connection.

Generally, measuring the full 3D radiation pattern of the RF probe-fed mm-wave antenna is challenging due to obstruction of the probe and the probe station [57], [58]. The probe blocks a part of the measured radiation pattern and limits the dynamic range due to its unwanted radiation [59]–[61]. The unwanted radiation can occur at the transition from the RF probe to the transmission line, and on the edge of the PCB due to diffraction and reflections from, for example, the housing of the RF probe or the connector. In all cases, this unwanted radiation will influence the radiation pattern and the antenna gain. Additionally, the metal surface of the probe station could cause a reflection that results in a ripple on the radiation pattern.

To mitigate the undesired interference and improve measurement uncertainty, RF probe-fed measurement techniques can be broadly characterized into two categories, that is, error compensation through postprocessing approaches, and a modified measurement setup [53]. The former can be estimated using superposition and S-parameter techniques to de-embed parasitic probe radiation [53]. It can also be estimated by using load subtraction and modal filtering to separate the probe radiation. For the latter, modification of the measurement setup is commonly done by displacing the probe positioner out of the anechoic chamber, or by covering it with an absorber [62]. However, it should be done with caution so that the absorber does not influence the antenna. In [57], the measurement is done quasi-in-the-air to avoid metal reflections. Meanwhile, in [59] and [63], the unwanted radiation of the probe is reflected out of the probe station by putting a metal plate behind the probe, but the measurement aperture is narrowed.

Additionally, a special holder is used to hold the DUT. To avoid unwanted reflection from the metallic surface and dielectric materials are used as the DUT holder [64], [65]. Custom probes with extended and bent probe tips are proposed to avoid blockage from the fixture [58]. However, custom probes can have a higher insertion loss, making calibration especially challenging for terahertz (THz) frequencies. The insertion loss of the probe cannot always be neglected, and

TABLE 4. THE ADVANTAGES AND DISADVANTAGES OF A MIDFIELD SYSTEM.

Advantages	Disadvantages
• smaller distance than a DFF • measures continuous-wave and modulated signals.	• requires error-correction process • accurate only for beam peaks.

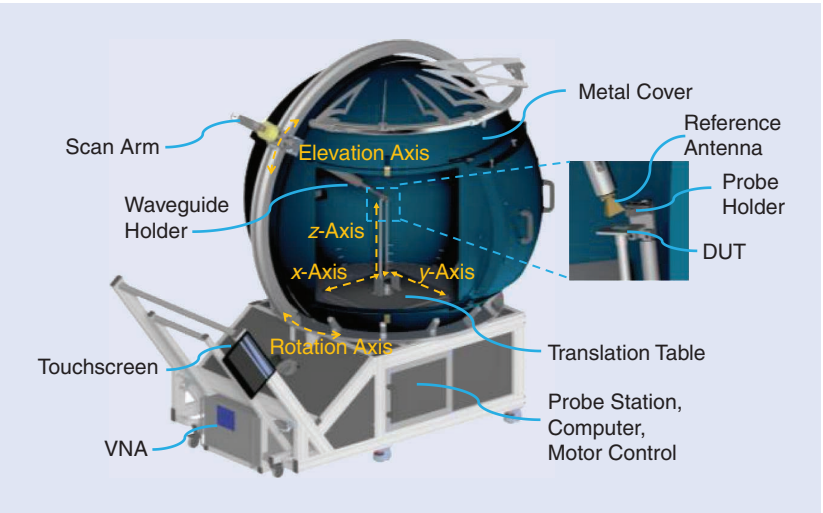

FIGURE 7. The compact portable mm-wave anechoic chamber at Eindhoven University of Technology.

it can be analyzed using a back-to-back probe test [66].

Systematic errors of the cable and the probe itself can be de-embedded using a planar calibration substrate [67]. However, the calibration procedure is not so straightforward. One of the challenges is to correctly land all probe pins on the calibration substrate. An incorrect connection between the probe and the calibration substrate leads to undesired radiation from the probe due to the coupling between the probe tip and the substrate. In [68], an automatic probing algorithm is applied to improve repeatability of the probe position.

The NF scan for a probe-fed antenna is performed in [58] and [69]. However, the NF scanning range is also limited by the size of the probe. This makes the measurement of an antenna with a wide beamwidth not possible. In [70], a robotic positioning system with a laser tracker feature is used to improve the flexibility of a spherical NF measurement system. However, the robot movement is still limited to measure the lower hemisphere. The estimated measurement result in this area is calculated by mirroring the measured field in the upper hemisphere, increasing the uncertainty of the result [70]. Moreover, use of the robotic arm for the probe-fed antenna measurement cannot largely improve the overall uncertainty as the largest error contributor is from the probe effects. Recently, the probe-fed antenna measurement technique using the IFF method was applied to measure the beamforming capabilities of a 5G mm-wave AiP [18]. The advantages and disadvantages of the RF probe-fed measurement system are summarized in Table 5.

The phase center is the specific reference point in the antenna (assumed point source) from which the radiation may originate.

3GPP UNCERTAINTY ASSESSMENT OF OTA SYSTEMS

Any measurement, including an OTA one, is subject to errors that affect measurement results. To determine measurement uncertainty, an uncertainty budget containing the factors and their contributions should be defined [71]. The uncertainty assessments for 5G mm-wave UE and base station measurements using different OTA methods have been published by the 3GPP [6], [72]. This section gives a practical interpretation of what the 3GPP defines.

Table 6 lists the 3GPP uncertainty assessment for an EIRP measurement using DFF, IFF (CATR), and NF measurement systems at 28 GHz [6]. The standard uncertainty in Table 6 is generally based on the measurement performed by the 3GPP for assessment of the uncertainty. The assessment for DFF and NF are performed with the 5-cm DUT, while for IFF with a 15-cm DUT.

An analysis is done for two stages of measurement (a gain-comparison method), as illustrated in Figure 8. The uncertainty contributors of each stage are added in the figure. At the first stage, a calibration of the absolute level of the DUT measurement results is performed using a reference antenna, whose absolute gain is known. The reference antenna is measured in the same place as the DUT to calibrate the path loss. At the second stage, the actual measurement with the DUT as either the transmitter or receiver is performed.

Table 6 shows that DFF has the largest overall uncertainty, whereas NF has the smallest of all the methods. The expanded uncertainties are obtained by calculating the root sum of squares of the combined standard uncertainties with a 95% confidence (k = 2). The largest uncertainty is from the quality of the quiet zone that quantifies the effect of reflections within the anechoic chamber (see numbers 1 and 10 in Table 6). To evaluate the quality of the quiet zone, an antenna pattern comparison and free-space voltage standing-wave ratio field probe techniques are frequently used [73]. They can predict the variation of measurement results when the DUT is placed anywhere within the quiet zone, and with the beam formed in any direction. The evaluated area mainly depends on the size and the minimum FF distance of the DUT. However, the result of the procedures is greatly affected by directivity of the probe antenna itself [73].

The second-largest uncertainty is caused by a mismatch from the nonideal matching of the connected instruments, as shown in number 11 in Table 6. This term can be calculated from the reflection coefficients at the generator and the receiving device. This term can be largely calibrated out, for example, by using a two-port VNA calibration. Moreover, any components added to the measurement setup can contribute to measurement uncertainty, thus, the uncertainty contributed from that component should be identified. For the case of an external amplifier, an uncertainty of 1 dB is contributed due to its instability and nonlinearity, as shown in number 13 in Table 6.

The absolute antenna gain uncertainty of the calibration antenna (see number 2 in Table 6) originates from the calibration measurement in "Stage 1: Calibration." The uncertainty can be obtained using Type B uncertainty

TABLE 5. THE ADVANTAGES AND DISADVANTAGES OF AN RF PROBE-FED MEASUREMENT.

Advantages	Disadvantages
• possible to measure integrated antennas	• unwanted radiation at probe-antenna transition
• flexible probing and placement	• probe-tip damage
• no mechanical stress due to RF cable	• repeatability of calibration
• simple interface design on the PCB for interconnection setting.	• increased uncertainty of calibration.

analysis from the calibration report with traceability to a national metrology institute. The uncertainty of the network analyzer and RF power measurement equipment (see numbers 3 and 12 in Table 6) could also be obtained using Type B uncertainty analysis from the manufacturer's data sheet. It needs to be ensured that appropriate uncertainty contributions are specified for the settings used, such as bandwidth and absolute level.

The random uncertainty (see number 14 in Table 6) is due to the unknown and unquantifiable uncertainties associated with the measurements that cannot be measured and reduced completely. The random uncertainty of the 4G LTE OTA measurements is defined to be approximately 0.2 dB [6]. This value is increased for an mm-wave system (see number 14 in Table 6) due to increased sensitivity to random effects in more complex, higher-frequency NR test systems.

In the following section, the uncertainties specific to each measurement system are described.

MEASUREMENT UNCERTAINTY OF DFF METHODS

For measurements using the DFF method, the uncertainty contributors in two stages of the 3GPP uncertainty assessment are illustrated in Figure 8. The measurement distance uncertainty is one of the largest uncertainty contributors for the DFF (see number 17 in Table 6) [6]. This is shown in "Stage 2—DUT Measurement" in Figure 8. For radiation pattern measurement, the finite measurement distance affects characterization of the sidelobe and

TABLE 6. THE 3GPP UNCERTAINTY ASSESSMENT FOR AN EIRP MEASUREMENT USING DFF, IFF, AND NF MEASUREMENT SYSTEMS.

		Standard Uncertainty		
No.	**Uncertainty Source**	**DFF (dB)**	**IFF (dB)**	**NF (dB)**
	Stage 1: Calibration			
1	Quality of the quiet zone	1.5	1.5	1.5
2	Uncertainty of an absolute gain of the calibration antenna	0.8	0.8	0.8
3	Uncertainty of the network analyzer	0.2	0.2	0.21
4	Positioning and pointing misalignment between the reference and receiving antennas	0.2	0.05	—
5	Phase-center offset of the calibration antenna	0.36	—	—
6	Reference antenna feed cable loss measurement uncertainty	0.17	—	—
7	Reference antenna positioning misalignment	0.17	—	—
8	Mismatch in the connection of the calibration antenna	—	0.05	0.07
9	RF leakage (from the measurement antenna to the receiver)	—	0.1	—
	Stage 2: DUT Measurement			
10	Quality of the quiet zone	1.5	1.5	1.5
11	Mismatch	1.3	1.3	1.3
12	Uncertainty of the RF power measurement equipment	1.08	1.08	1.08
13	Amplifier uncertainty	1	1	1
14	Random uncertainty	0.23	0.23	0.23
15	Influence of the XPD	0.48	0.48	—
16	Positioning misalignment	0.29	0.05	—
17	Measurement distance uncertainty	0.58	—	—
18	RF leakage (from the measurement antenna to the receiver)	—	0.1	—
19	Insertion-loss variation of the receiver chain	—	0.06	—
20	Phase drift and noise	—	—	0.02
21	NF-to-FF truncation	—	—	0.003
22	Probe-polarization amplitude and phase	—	—	0.055
Expanded uncertainty (95% confidence interval)		**6.2**	**5.99**	**5.19**

XPD: cross-polar discrimination.

nulls. The distance should be large enough to avoid any mutual coupling between the antennas and errors from the phase taper [64]. However, expanding the distance increases the FSPL and cable losses, which reduces the signal-to-noise ratio. Uncertainty of the distance-measuring tool also needs to be determined and accounted for.

Additionally, the result could vary with changes in the distance if the phase center of the antenna is unknown [74]. The phase center is the specific reference point in the antenna (assumed point source) from which the radiation may originate. However, the distance is usually incorrectly defined from the antenna aperture, which is easier to be measured. If the phase center of the antenna is not aligned with the center coordinate of measurement, there is an additional uncertainty related to the measurement distance, which decreases as the measurement distance increases. Therefore, the uncertainty of this point should be analyzed by considering the area between the feed and aperture of antennas [75]. This contributes to roughly 0.36 dB of the uncertainty budget (see number 5 in Table 6) [6]. To reduce uncertainty due to the phase center, a simulation and a prior calculation are proposed to find the phase center of the antenna [76]. Moreover, instead of using a phase center, van den Biggelaar [14] uses an amplitude center to confirm that the FF condition is met. Another approach is to implement an extrapolation measurement technique [77] or a gain-correction factor [78]. The former uses Wacker's equation to model the interaction between two antennas, while the latter is estimated by taking the ratio between the finite-range and FF gain.

For IFF measurements using the CATR system, quality of the quiet zone is also the largest uncertainty contributor in the system.

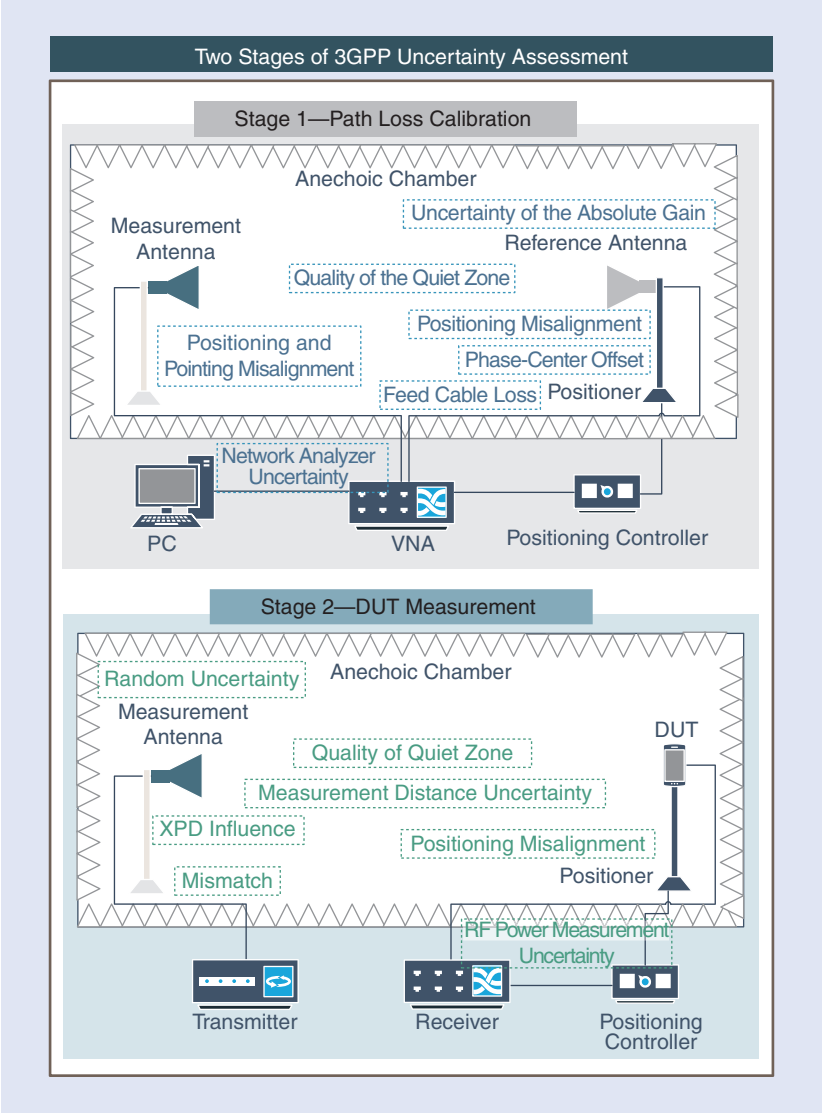

FIGURE 8. The two stages of 3GPP uncertainty assessments for a DFF measurement with the uncertainty contributors. Stage 1—path loss calibration. Stage 2—the DUT measurement. XPD: cross-polar discrimination.

The positioning misalignment contributes to the measurement in both stages (see numbers 4 and 16 in Table 6). In the measurement in "Stage 1: Calibration," it originates from the reference antenna alignment and pointing errors (see Figure 8). In this measurement, if the maximum gain directions of the reference antenna and the receiving antenna are aligned, the contribution can be considered negligible. In "Stage 2—DUT Measurement," it originates from misalignment of the transmitting and receiving antennas (see Figure 8). The uncertainty is caused by misalignment of the testing and the beam-peak direction of the receiving antenna due to rotation system errors. The effect of the misalignment depends highly on the beamwidth of the beam under test. For devices with a narrow beamwidth, this uncertainty leads to a larger measurement error.

To validate the alignment and position of the antennas, an alignment camera can be used for tracking by adding a marking on the antennas [79]. Another approach is to use a laser tracker [80]. A laser generator is positioned between both antennas, and the horizontal and vertical position of the antenna can be adjusted using the

mark from the laser beam. In addition, to ensure that the cable's position and bendablility are repeatable, cable supports can be added to the antenna carrier to avoid phase deviations among various measurements [81].

To increase flexibility of the movement, the use of a robotic arm has been proposed in [60] and [82]. The antenna alignment and positioning are dynamically monitored for the uncertainty analysis; however, the positioning depends on the speed and acceleration of the robot. It also has uncertainty due to cable movement and noise of the robot [60].

If the measurement is performed using a dual-polarized probe, as it was done for the DFF and IFF assessments in Table 6 [6], the uncertainty caused due to the finite cross-polar discrimination (XPD) between the two polarization ports should be accounted for (see number 15 in Table 6). A typical probe antenna can have an XPD of 30 dB [6].

MEASUREMENT UNCERTAINTY OF IFF METHODS

For IFF measurements using the CATR system, quality of the quiet zone is also the largest uncertainty contributor in the system (see numbers 1 and 10 in Table 6). This could be improved by implementing an edge treatment on the parabolic reflector. If the reflector has a simple parabolic shape with sharp edges, the diffraction could result in a ripple in the quiet zone. The edges can be serrated and rolled to scatter energy away from the quiet zone. This reflector is used for an OTA measurement of the mm-wave base station in [83].

The pointing and positioning misalignment uncertainty of IFF is smaller than that of DFF (see numbers 4 and 16 in Table 6). The contribution of pointing misalignment of IFF originates from uncertainty in the sliding position and the turntable angle. If the calibration antenna is aligned to its beam peak, this contribution can be considered negligible and therefore set to zero.

From the 3GPP assessment depicted in Table 6, other uncertainty contributors are from the RF equipment (see number 18 in Table 6), such as insertion-loss variation of the receiver chain and RF leakage [6]. Uncertainty from the insertion-loss variation of the receiver chain is the residual uncertainty contribution coming from introducing an antenna at the end of the cable. If this cable does not change or move between the two stages, the uncertainty is assumed to be systematic and negligible during the measurement stage.

RF leakage from the measurement antenna to the receiver or the transmitter denotes noise leaking into the connector and cables between the measurement antenna and the receiving or transmitting equipment. This contribution also includes the noise leakage between the connector and cables between the reference antenna and transmitting equipment for the calibration phase.

MEASUREMENT UNCERTAINTY OF NF METHODS

For NF measurements, the measured NF is expanded using a finite set of spherical modes linked to the number of samples. The filtering effect generated by the finite number of modes can improve measurement results by removing signals from outside the physical area of the DUT. However, care must be taken to make sure that the removed signals are not from the DUT itself or it will cause truncation of NF to FF. The uncertainty of NF-to-FF truncation (see number 21 in Table 6) includes the uncertainty related to the scan-area truncation.

The uncertainty of the phase drift and noise is due to the noise level and drift of the test range and should be determined at the DUT location. The noise level is usually measured with a spectrum analyzer. The amplitude and phase of the probe-polarization coefficients should be measured. If the probe-polarization amplitude and phase are measured and corrected for, then the probe XPD uncertainty term can be negligible.

The filtering effect generated by the finite number of modes can improve measurement results by removing signals from outside the physical area of the DUT.

For spherical NF scanning, the error terms and measurement uncertainty are analyzed in [84]–[87]. The method of estimating uncertainties due to multiple reflections between the probe and test antennas in NF measurements is presented in [85]. In [86], the antenna pattern comparison approach is used to estimate error terms from the multiple reflections, probe alignment, and probe-position error. In [87], the measurement error due to mechanical uncertainties for planar and spherical scanning in THz frequencies is observed. It is found that the error levels converge to increasing measurement distances for those of spherical systems.

Recently, the effect of probe imperfection on measurement uncertainty was investigated by modeling the spherical NF system configuration in a full-wave simulation [88]. Simulations of chambers and NF systems are performed to approximate the error from the chamber's stray signals and misalignment of the probe and DUT movements. In the future, measurement uncertainty can be estimated based on not only measurement data but also on simulation ones due to improvements in simulation computations of antenna system modeling.

MEASUREMENT UNCERTAINTY OF MIDFIELD METHODS

Kong et al. [15] claimed that the measurement uncertainty of midfield measurements is the same as that for DFF for some metrics, such as for TRP. Therefore, the 3GPP assessment of DFF measurement uncertainty can be referred directly for midfield uncertainty analysis. However, for beam-peak direction metrics such as EIRP and EIS, a correction factor is applied to the midfield measurement results to get the FF result [15]. The correction factor

TABLE 7. A COMPARISON OF OTA MEASUREMENT SYSTEMS.

Parameter	DFF	CATR	NF			Midfield
			Planar	Cylindrical	Spherical	
Minimum distance	$\frac{2D^2}{\lambda}$	3.5 × reflector size		3λ		$\frac{0.5D^2}{\lambda}$ *
Setup complexity	Simple	Complex		Medium	Complex	Simple
Measured signals	Continuous wave, modulated	Continuous wave, modulated		Continuous wave		Continuous wave, modulated

*Based on the calculation for a 15-cm device at 43 GHz [30].

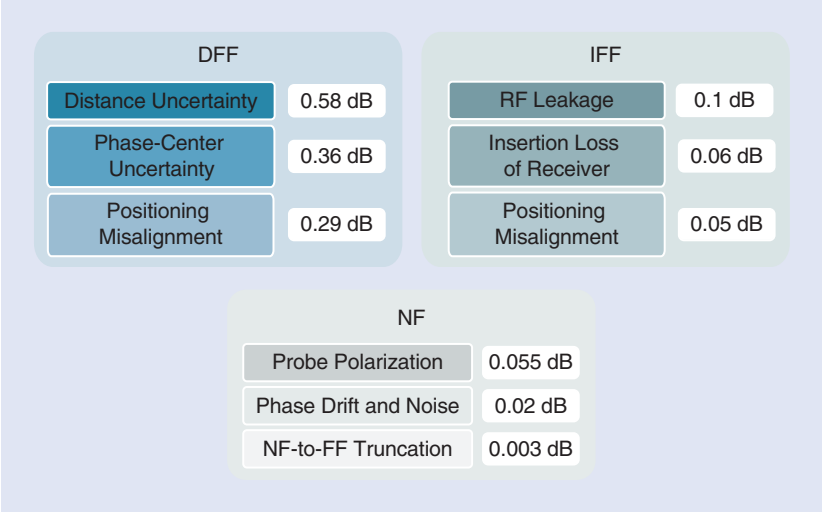

FIGURE 9. The specific uncertainty contributors of DFF, IFF, and NF measurements based on a 3GPP assessment.

introduces a new contributor to the measurement uncertainty, which makes the uncertainty of the midfield measurement system slightly larger than the DFF.

Additionally, as the distance between the probe and the DUT is shorter, the uncertainty of the phase-center offset and the longitudinal taper error is increased. This contributes to additional uncertainty for the radiation pattern measurement of the main beam (EIRP and EIS). For example, for a 72-mm DUT operating at 43.5 GHz measured with 50-cm distances, an error of approximately 1.25 dB is added, which mostly affects the second lobes [16]. The measurement of TRP with this method also deviates in roughly the same order [16].

CONCLUSIONS

In this article, an overview of integrated-antenna OTA test systems for 5G-and-beyond mm-wave applications was given. A comparison of each measurement system is shown in Table 7, and the specific uncertainty contributors based on the 3GPP assessment are presented in Figure 9. By considering the significant parameters, including the measurement distance, complexity of the setup configuration, desired metrics, and uncertainty contributors of each system, a framework was provided to select the most suitable OTA measurement method for a particular integrated antenna. Tradeoffs between the complexity of the electrical and mechanical components, the desired metrics that need to be evaluated, and the uncertainty of the measurement may be necessary. As a result, a single OTA solution may not be the most practical and ideal option for all integrated antenna measurements for mm-wave applications. Therefore, the reader should decide which measurement methods are suitable for their measurement facility based on the described factors in this article. Furthermore, the techniques that reduce the uncertainty of an OTA measurement for mm-wave or even THz communication for 5G-and-beyond applications are an ongoing challenge for the measurement community.

ACKNOWLEDGMENT

The authors thank National Instruments, in particular, Marc van den Bossche and Jan Fromme for their support and funding, which made this research possible.

AUTHOR INFORMATION

Imee Ristika Rahmi Barani (imee.barani@antennacompany.com) is with the Antenna Company, 5656 AE Eindhoven, The Netherlands. Her research interests include low-profile multiple-input, multiple-output antenna designs for wireless communication devices and antenna metrology. She is a Member of IEEE.

Laurens A. Bronckers (l.a.bronckers@tue.nl) is with the Electromagnetics Group, Department of Electrical Engineering, Eindhoven University of Technology, 5600 MB Eindhoven, The Netherlands. He is an assistant professor in metrology for antennas and wireless systems. His research interests include (millimeter-wave) measurements using reverberation chambers, channel emulation, and channel sounding. He is a Member of IEEE.

Adrianus C.F. Reniers (a.reniers@tue.nl) is with the Electromagnetics Group, Department of Electrical Engineering, Eindhoven University of Technology, 5600 MB Eindhoven, The Netherlands. His research topic is

metrology for antennas and wireless systems. His research interests include (millimeter-wave) measurements using anechoic chambers with both NF and FF capabilities. He is a Member of IEEE.

REFERENCES

[1] J. G. Andrews et al., "Modeling and analyzing millimeter wave cellular systems," *IEEE Trans. Commun.*, vol. 65, no. 1, pp. 403–430, Jan. 2017, doi: 10.1109/TCOMM.2016.2618794.

[2] A. C. F. Reniers, U. Johannsen, and A. B. Smolders, "Antenna-in-package measurements," in *Antenna-in-Package Technology and Applications*, D. Liu and Y. Zhang, Eds. Hoboken, NJ, USA: Wiley, 2020, p. 11.

[3] W. Fan et al., "A step toward 5G in 2020: Low-cost OTA performance evaluation of massive MIMO base stations," *IEEE Antennas Propag. Mag.*, vol. 59, no. 1, pp. 38–47, Feb. 2017, doi: 10.1109/MAP.2016.2630020.

[4] "Universal mobile telecommunications system (UMTS); LTE; universal terrestrial radio access (UTRA) and evolved universal terrestrial radio access (E-UTRA); verification of radiated multi-antenna reception performance of user equipment (UE)," 3GPP, Sophia Antipolis, France, TR 37.977 v12.0.0, 2014.

[5] "Test plan for 2 × 2 downlink MIMO and transmit diversity over-the-air performance," CTIA, Washington, DC, USA, Revision 1.1, Aug. 2016.

[6] "Technical Specification Group Radio Access Network; NR; Study on test methods," 3GPP, Sophia Antipolis, France, TR 38.810 v16.5.0, 2019.

[7] Y. Jing, H. Kong, and M. Rumney, "MIMO OTA test for a mobile station performance evaluation," *IEEE Instrum. Meas. Mag.*, vol. 19, no. 3, pp. 43–50, Jun. 2016, doi: 10.1109/MIM.2016.7477954.

[8] Y. Jing, M. Rumney, H. Kong, and Z. Wen, "Overview of 5G UE OTA performance test challenges and methods," in *Proc. 2018 IEEE MTT-S Int. Wireless Symp. (IWS)*, Chengdu, pp. 1–4, doi: 10.1109/IEEE-IWS.2018.8400996.

[9] Y. Qi et al., "5G over-the-air measurement challenges: Overview," *IEEE Trans. Electromagn. Compat.*, vol. 59, no. 6, pp. 1661–1670, Dec. 2017, doi: 10.1109/TEMC.2017.2707471.

[10] S. G. Pannala, "Feasibility and challenges of over-the-air testing for 5G millimeter wave devices," in *Proc. 2018 IEEE 5G World Forum (5GWF)*, Silicon Valley, CA, USA, pp. 304–310, doi: 10.1109/5GWF.2018.8516965.

[11] M. D. Foegelle, "New and continuing measurement challenges for 5g mmwave and beamforming technologies," in *Proc. 2019 13th Eur. Conf. Antennas Propag. (EuCAP)*, Krakow, Poland, pp. 1–5.

[12] G. F. Masters, "An introduction to mobile station over-the-air measurements," in *Proc. Antenna Meas. Techn. Assoc.*, 2006, pp. 237–242.

[13] C. Parini, S. Gregson, J. McCormick, and D. J. van Rensburg, *Theory and Practice of Modern Antenna Range Measurements*. London, U.K.: The IET, 2014.

[14] A. J. T. van den Biggelaar, "Over-the-air characterization of millimeter-wave integrated antenna systems," Ph.D. dissertation, Technische Universiteit Eindhoven, Eindhoven, The Netherlands, 2020.

[15] H. Kong, Z. Wen, Y. Jing, and M. Yau, "Mid-field over-the-air test: A new OTA RF performance test method for 5G massive MIMO devices," *IEEE Trans. Microw. Theory Techn.*, vol. 67, no. 7, pp. 2873–2883, Jul. 2019, doi: 10.1109/TMTT.2019.2912369.

[16] B. Derat, G. F. Hamberger, and F. Michaelsen, "On the minimum range length for performing accurate direct far-field over-the-air measurements," in *Proc. 2019 Antenna Meas. Techn. Assoc. Symp. (AMTA)*, San Diego, CA, USA, pp. 1–5, doi: 10.23919/AMTAP.2019.8906460.

[17] G. F. Hamberger, C. Rowell, and B. Derat, "Near-Field Techniques for Millimeter-Wave Antenna Array Calibration," in *Proc. 2019 Antenna Meas. Techn. Assoc. Symp. (AMTA)*, San Diego, CA, USA, pp. 1–5, doi: 10.23919/AMTAP.2019.8906415.

[18] S.-C. Hsieh, F.-C. Chu, C.-Y. Ho, W.-Y. Chen, and C.-C. Wang, "mmWave AiP measurement turnkey solution in millimeter-wave wireless communication applications," in *Proc. 2020 IEEE 70th Electron. Compon. Technol. Conf. (ECTC)*, Orlando, FL, USA, pp. 114–119, doi: 10.1109/ECTC32862.2020.00031.

[19] C. A. Balanis, *Antenna Theory: Analysis and Design*. Hoboken, NJ, USA: Wiley, 2016.

[20] M. Jacob, T. Marshall, C. Coleman, M. Rumney, P. Ramachandran, and G. VanWiggeren, "Characterization challenges for millimeter-wave multi-antenna 5G devices," in *Proc. 12th Eur. Conf. Antennas Propag. (EuCAP 2018)*, London, U.K., 2018, pp. 1–4, doi: 10.1049/cp.2018.0857.

[21] R. Johnson, H. Ecker, and R. Moore, "Compact range techniques and measurements," *IEEE Trans. Antennas Propag.*, vol. 17, no. 5, pp. 568–576, Sep. 1969, doi: 10.1109/TAP.1969.1139517.

[22] Z. N. Chen, *Handbook of Antenna Technologies*. Singapore: Springer Singapore, 2016.

[23] J. Yu et al., "The design and manufacture of a high frequency CATR," in *Proc. 2013 6th U.K., Europe, China Millimeter Waves THz Technol. Workshop (UCMMT)*, Rome, Italy, pp. 1–2, doi: 10.1109/UCMMT.2013.6641506.

[24] M. Paquay, L. S. Drioli, L. Rolo, X. Allart, and E. Saenz, "Quiet zone characterisation at mm-wave frequencies in CATR's," in *Proc. 2009 3rd Eur. Conf. Antennas Propag.*, Berlin, pp. 929–933.

[25] B. Derat, C. Rowell, and A. Tankielun, "Promises of near-field software and hardware transformations for 5G OTA," in *Proc. 2018 IEEE Conf. Antenna Meas. Appl. (CAMA)*, Vasteras, pp. 1–4, doi: 10.1109/CAMA.2018.8530646.

[26] H. F. Schluper, J. Van Damme, and V. J. Vokurka, "Optimized collimators—theoretical performance limits," in *Proc. Antenna Meas. Techn. Assoc.*, Seattle, WA, USA, Oct. 1987, p. 313.

[27] Z. Li, J. Wu, D. Xu, G. Zhou, J. Zhao, and G. He, "Design and realization of a small compact antenna test range at low frequency," in *Proc. Antenna Meas. Techn. Assoc.*, Seattle, WA, USA, Oct. 2015.

[28] L. J. Foged, A. Riccardi and A. Giacomini, "Numerical investigation of cross polar reduction CATR feed in dual linear polarization," in *Proc. 2016 IEEE Int. Symp. Antennas Propag. (APSURSI)*, Fajardo, pp. 1621–1622.

[29] M. Multari et al., "77 GHz stepped lens with sectorial radiation pattern as primary feed of a lens based CATR," *IEEE Trans. Antennas Propag.*, vol. 58, no. 1, pp. 207–211, Jan. 2010, doi: 10.1109/TAP.2009.2036130.

[30] T. Sehm, J. Ala-Laurinaho, T. Hirvonen, and A. V. Raisanen, "Antenna measurements using a hologram CATR," *Electron. Lett.*, vol. 35, no. 10, pp. 757–758, May 13, 1999, doi: 10.1049/el:19990557.

[31] Z. P. Li, J. Ala-Laurinaho, Z. Du, and A. V. Räisänen, "Realization of wideband hologram compact antenna test range by linearly adjusting the feed location," *IEEE Trans. Antennas Propag.*, vol. 62, no. 11, pp. 5628–5633, Nov. 2014, doi: 10.1109/TAP.2014.2351072.

[32] J. D. Kraus and R. J. Marhefka, *Antennas for All Applications*. New York, NY, USA: McGraw-Hill, 2003.

[33] *IEEE Draft Recommended Practice for Antenna Measurements*, IEEE P149/D11, Jul. 2021.

[34] Z. Li, P. Huo, Y. Wu, and J. Wu, "Reflectarray compact antenna test range with controlled aperture disturbance fields," *IEEE Antennas Wireless Propag. Lett.*, vol. 20, no. 7, pp. 1283–1287, Jul. 2021, doi: 10.1109/LAWP.2021.3077739.

[35] P. E. Schoessow, "Plane wave synthesis a new approach to the problem on antenna near-field/far-field transformation," Ph.D. dissertation, Dept. Elect. Eng., Univ. Sheffield, Sheffield, U.K., 1981.

[36] A. Scannavini, F. Saccardi, L. J. Foged, and K. Zhao, "Impact of Phase Curvature on Measuring 5G Millimeter Wave Devices," in *Proc. 2019 Antenna Meas. Techn. Assoc. Symp. (AMTA)*, San Diego, CA, USA, pp. 1–4, doi: 10.23919/AMTAP.2019.8906462.

[37] Y. Wu, J. Wu, and Z. Li, "Plane wave synthesis using near field wave spectrum transform embedded into intersection approach," in *Proc. Int. Conf. Microw. Millimeter Wave Technol. (ICMMT)*, 2018, pp. 1–3, doi: 10.1109/ICMMT.2018.8563534.

[38] A. Yaghjian, "An overview of near-field antenna measurements," *IEEE Trans. Antennas Propag.*, vol. 34, no. 1, pp. 30–45, Jan. 1986, doi: 10.1109/TAP.1986.1143727.

[39] *IEEE Recommended Practice for Near-Field Antenna Measurements*, IEEE Standard 1720-2012.

[40] S. F. Razavi and Y. Rahmat-Samii, "Resilience to probe-positioning errors in planar phaseless near-field measurements," *IEEE Trans. Antennas Propag.*, vol. 58, no. 8, pp. 2632–2640, Aug. 2010, doi: 10.1109/TAP.2010.2050421.

[41] S. F. Gregson and Z. Tian, "Comparison of spherical and cylindrical mode filtering techniques for reflection suppression with mm-wave antenna measurements," in *Proc. 2018 IEEE Conf. Antenna Meas. Appl. (CAMA)*, Vasteras, pp. 1–4, doi: 10.1109/CAMA.2018.8530460.

[42] P. Petre and T. K. Sarkar, "Planar near-field to far-field transformation using an equivalent magnetic current approach," *IEEE Trans. Antennas Propag.*, vol. 40, no. 11, pp. 1348–1356, Nov. 1992, doi: 10.1109/8.202712.

[43] S. F. Gregson, C. G. Parini, and J. McCormick, "Development of wide-angle pattern measurements using a probe-corrected polyplanar near-field measurement technique," *Inst. Elect. Eng. Proc. Microw. Antennas Propag.*, vol. 152, no. 6, pp. 563–572, Dec. 2015, doi: 10.1049/ip-map:20045157.

[44] E. Martini, O. Breinbjerg, and S. Maci, "Reduction of truncation errors in planar near-field aperture antenna measurements using the Gerchberg-Papoulis algorithm," *IEEE Trans. Antennas Propag.*, vol. 56, no. 11, pp. 3485–3493, Nov. 2008, doi: 10.1109/TAP.2008.2005442.

[45] P. O. Iversen, P. Garreau, and D. Burrell, "Real-time spherical near-field handset antenna measurements," *IEEE Antennas Propag. Mag.*, vol. 43, no. 3, pp. 90–94, Jun. 2001, doi: 10.1109/74.934906.

[46] A. Arboleya, Y. Álvarez, and F. Las-Heras, "Millimeter and submillimeter planar measurement setup," in *Proc. 2013 IEEE Antennas Propag. Soc. Int. Symp. (APSURSI)*, Orlando, FL, USA, pp. 1–2, doi: 10.1109/APS.2013.6710661.

[47] Y. Rahmat-Samii and S. F. Razavi, "The art and engineering of modern antenna near-field measurements," in *Proc. 2009 SBMO/IEEE MTT-S Int. Microw. Optoelectron. Conf. (IMOC)*, Belem, pp. 344–349, doi: 10.1109/IMOC.2009.5427567.
[48] A. Arboleya et al., "Phaseless characterization of broadband antennas," *IEEE Trans. Antennas Propag.*, vol. 64, no. 2, pp. 484–495, Feb. 2016, doi: 10.1109/TAP.2015.2511789.
[49] P. Huo, J. Wu, Z. Wang, and Z. Li, "Digital holographic reconstruction and filtering method for antenna planar near-field phase-less measurement," *IEEE Antennas Wireless Propag. Lett.*, vol. 16, pp. 2927–2930, Sep. 2017, doi: 10.1109/LAWP.2017.2752898.
[50] B. Derat, G. F. Hamberger, and F. Michaelsen, "Shortest range length to measure the total radiated power," *IET Microw., Antennas Propag.*, vol. 13, no. 15, pp. 2584–2589, Dec. 18, 2019, doi: 10.1049/iet-map.2019.0408.
[51] H. Kong, Y. Jing, Z. Wen, and L. Cao, "Mid-field OTA RF test method: new developments and performance comparison with the compact antenna test range (CATR)," in *Proc. 2020 14th Eur. Conf. Antennas Propag. (EuCAP)*, Copenhagen, Denmark, pp. 1–5, doi: 10.23919/EuCAP48036.2020.9135921.
[52] R. N. Simons and R. Q. Lee, "On-wafer characterization of millimeter-wave antennas for wireless applications," *IEEE Trans. Microw. Theory Techn.*, vol. 47, no. 1, pp. 92–96, Jan. 1999, doi: 10.1109/22.740086.
[53] M. R. Karim, X. Yang, and M. F. Shafique, "On chip antenna measurement: A survey of challenges and recent trends," *IEEE Access*, vol. 6, pp. 20,320–20,333, Mar. 2018, doi: 10.1109/ACCESS.2018.2821196.
[54] A. C. F. Reniers, A. R. van Dommele, A. B. Smolders, and M. H. A. J. Herben, "The influence of the probe connection on mm-wave antenna measurements," *IEEE Trans. Antennas Propag.*, vol. 63, no. 9, pp. 3819–3825, Sep. 2015, doi: 10.1109/TAP.2015.2452941.
[55] A. C. F. Reniers, Q. Liu, M. H. A. J. Herben and A. B. Smolders, "Review of the accuracy and precision of mm-wave antenna simulations and measurements," in *Proc. 2016 10th Eur. Conf. Antennas Propag. (EuCAP)*, Davos, pp. 1–5, doi: 10.1109/EuCAP.2016.7481973.
[56] A. C. F. Reniers and A. B. Smolders, "Guidelines for millimeter-wave antenna measurements," in *Proc. 2018 IEEE Conf. Antenna Meas. Appl. (CAMA)*, Vasteras, pp. 1–4, doi: 10.1109/CAMA.2018.8530518.
[57] S. Ranvier, M. Kyrö, C. Icheln, C. Luxey, R. Staraj, and P. Vainikainen, "Compact 3-D on-wafer radiation pattern measurement system for 60 GHz antennas," *Microw. Opt. Technol. Lett.*, vol. 51, no. 2, pp. 319–324, 2009, doi: 10.1002/mop.24034.
[58] S. Beer and T. Zwick, "Probe based radiation pattern measurements for highly integrated millimeter-wave antennas," in *Proc. 4th Eur. Conf. Antennas Propag.*, Barcelona, 2010, pp. 1–5.
[59] Z. Tsai, Y. Wu, S. Chen, T. Lee, and H. Wang, "A V-band on-wafer near-field antenna measurement system using an IC probe station," *IEEE Trans. Antennas Propag.*, vol. 61, no. 4, pp. 2058–2067, Apr. 2013, doi: 10.1109/TAP.2012.2237091.
[60] K. Mohammadpour-Aghdam, S. Brebels, A. Enayati, A. R. Faraji-Dana, G. A. E. Vandenbosch, and W. DeRaedt, "RF probe influence study in millimeter-wave antenna pattern measurements," *Int J RF Microw. Comput.-Aided Eng.*, vol. 21, no. 4, pp. 413–420, 2011, doi: 10.1002/mmce.20530.
[61] J. Murdock, E. Ben-Dor, F. Gutierrez, and T. S. Rappaport, "Challenges and approaches to on-chip millimeter wave antenna pattern measurements," in *Proc. 2011 IEEE MTT-S Int. Microw. Symp.*, Baltimore, MD, USA, pp. 1–4, doi: 10.1109/MWSYM.2011.5972965.
[62] T. Zwick, C. Baks, U. R. Pfeiffer, D. Liu, and B. P. Gaucher, "Probe based MMW antenna measurement setup," in *Proc. IEEE Antennas Propag. Soc. Symp.*, Monterey, CA, USA, 2004, vol. 1, pp. 747–750, doi: 10.1109/APS.2004.1329778.
[63] M. Mosalanejad, S. Brebels, I. Ocket, V. Volski, C. Soens, and G. A. E. Vandenbosch, "A complete measurement system for integrated antennas at millimeter wavelengths," in *Proc. 2015 9th Eur. Conf. Antennas Propag. (EuCAP)*, Lisbon, pp. 1–5.
[64] K. Van Caekenberghe et al., "A 2–40 GHz probe station based setup for on-wafer antenna measurements," *IEEE Trans. Antennas Propag.*, vol. 56, no. 10, pp. 3241–3247, Oct. 2008, doi: 10.1109/TAP.2008.929433.
[65] D. Titz, F. Ferrero, P. Brachat, G. Jacquemod, and C. Luxey, "Efficiency measurement of probe-fed antennas operating at millimeter-wave frequencies," *IEEE Antennas Wireless Propag. Lett.*, vol. 11, pp. 1194–1197, Oct. 2012, doi: 10.1109/LAWP.2012.2222336.
[66] Y. J. Shiao, J. Liao, and G. Huang, "On-wafer probes for submillimeter-wave on-chip antennas," in *Proc. 2015 IEEE MTT-S Int. Microw. Symp.*, Phoenix, AZ, USA, pp. 1–3, doi: 10.1109/MWSYM.2015.7167131.
[67] Q. Liu, A. C. F. Reniers, U. Johannsen, M. C. van Beurden, and A. B. Smolders, "Improved probing reliability in antenna-on-chip measurements," *IEEE Antennas Wireless Propag. Lett.*, vol. 17, no. 9, pp. 1745–1749, Sep. 2018, doi: 10.1109/LAWP.2018.2865605.
[68] R. Sakamaki and M. Horibe, "Long-term stability test on on-wafer measurement system in NMIJ," in *Proc. 2020 Conf. Precision Electromagn. Meas. (CPEM)*, Denver, CO, USA, pp. 1–2, doi: 10.1109/CPEM49742.2020.9191694.
[69] G. Gentile et al., "Silicon-filled rectangular waveguides and frequency scanning antennas for mm-wave integrated systems," *IEEE Trans. Antennas Propag.*, vol. 61, no. 12, pp. 5893–5901, Dec. 2013, doi: 10.1109/TAP.2013.2281518.
[70] L. Boehm, F. Boegelsack, M. Hitzler, and C. Waldschmidt, "The challenges of measuring integrated antennas at millimeter-wave frequencies [Measurements Corner]," *IEEE Antennas Propag. Mag.*, vol. 59, no. 4, pp. 84–92, Aug. 2017, doi: 10.1109/MAP.2017.2706652.
[71] "Joint Committee for Guides in Metrology," Bureau International des Poids et Mesures, Sèvres, France, 2012. Accessed: Nov. 2, 2020. [Online]. Available: https://www.bipm.org/utils/ common/documents/jcgm/JCGM_200_2012.pdf
[72] "Technical Specification Group Radio Access Network; Radio Frequency (RF) conformance testing background for radiated Base Station (BS) requirements," 3GPP, Sophia Antipolis, France, TR 37.941 V16.1.0, Sep. 2020.
[73] *IEEE Standard Test Procedures for Antennas*, ANSI/IEEE Standard 149-1979.
[74] K. Rutkowski and P. Iversen, "Methods to develop complete and accurate error budgets for antenna measurements," in *Proc. Antenna Meas. Tech. Assoc. Symp. (AMTA)*, Atlanta, GA, USA, Oct. 2010, pp. 394–400.
[75] S. Makoto, M. Hiroshi, F. Katsumi, S. Akira, K. Kunimasa, and Y. Yukio, "Evaluation of uncertainty of horn antenna calibration with the frequency range of 1 GHz to 18 GHz," *J. Nat. Inst. Inf. Commun. Technol.*, vol. 53, no. 1, pp. 29–42, 2006.
[76] E. G. Plaza, G. Leon, S. Loredo, and L. F. Herran, "Calculating the phase center of an antenna: a simple experimental method based on linear near-field measurements. [Measurements Corner]," *IEEE Antennas Propag. Mag.*, vol. 59, no. 5, pp. 130–175, Oct. 2017, doi: 10.1109/MAP.2017.2731209.
[77] A. J. Yuffa, "On Wacker's essential equation in the extrapolation measurement technique," in *Proc. 2019 Antenna Meas. Techn. Assoc. Symp. (AMTA)*, San Diego, CA, USA, pp. 1–5, doi: 10.23919/AMTAP.2019.8906417.
[78] T. S. Chu and R. A. Semplak, "Gain of electromagnetic horns," *Bell Syst. Tech. J.*, vol. 44, no. 3, pp. 527–537, Mar. 1965, doi: 10.1002/j.1538-7305.1965.tb01675.x.
[79] J. A. Gordon and D. R. Novotny, "Simultaneous imaging and precision alignment of two mm wave antennas based on polarization-selective machine-vision," *IEEE Trans. Instrum. Meas.*, vol. 61, no. 11, pp. 3065–3071, 2012, doi: 10.1109/TIM.2012.2202190.
[80] I. Expósito, M. García Sánchez, and I. Cuiñas, "Uncertainty assessment of a small rectangular anechoic chamber: From design to operation," *IEEE Trans. Antennas Propag.*, vol. 68, no. 6, pp. 4871–4880, Jun. 2020, doi: 10.1109/TAP.2020.2969842.
[81] A. Reniers, Q. Liu, M. Rousstia, M. Herben, H. Visser, and A. B. Smolders, "Statistical analysis applied to simulating and measuring circularly-polarized millimeter-wave antennas [Measurements Corner]," *IEEE Antennas Propag. Mag.*, vol. 61, no. 1, pp. 98–138, Feb. 2019, doi: 10.1109/MAP.2018.2883065.
[82] J. A. Gordon et al., "Millimeter-wave near-field measurements using coordinated robotics," *IEEE Trans. Antennas Propag.*, vol. 63, no. 12, pp. 5351–5362, 2015, doi: 10.1109/TAP.2015.2496110.
[83] L. M. Tancioni et al., "Over-the-air testing of active antenna system base stations in compact antenna test range," in *Proc. 2019 13th Eur. Conf. Antennas Propag. (EuCAP)*, Krakow, Poland, pp. 1–5.
[84] M. H. Francis and R. Wittmann, "Uncertainty analysis for spherical near-field measurements," in *Proc. Antenna Meas. Techn. Assoc. 2003*, Irvine, CA, USA, pp. 43–45.
[85] M. H. Francis, R. Wittmann, and J. S. Kang, "Uncertainties in spherical near-field antenna measurements," in *Proc. 2005 Int. Symp. Antennas Propag.*, Seoul, South Korea, pp. 273–276.
[86] G. Le Fur et al., "Uncertainty analysis of spherical near field antenna measurement system at VHF," in *Proc. Antenna Meas. Techn. Assoc.*, Tucson, AZ, USA, Oct. 2014.
[87] C. Culotta-López, R. Moch, R. Wilke, and D. Heberling, "On the influence of probe positioning errors due to mechanical uncertainties in spherical near-field measurements at terahertz frequencies in modern positioner systems," in *Proc. 2019 Photon. Electromagn. Res. Symp. - Spring*, pp. 1883–1888, doi: 10.1109/PIERS-Spring46901.2019.9017778.
[88] L. J. Foged, "Investigation of probe (IM) perfection vs measurement accuracy in spherical near-field systems," presented at the Antenna Measurement Techniques Association Regional Event, Apr. 22, 2021.